ACES Asian Chemical Editorial Society

DOI: 10.1002/asia.201600683

CHEMISTRY AN ASIAN JOURNAL Full Paper

Self-Assembly

Construction of Supramolecular Assemblies from Self-Organization of Amphiphilic Molecular Isomers

Zhaohua Li[+],[a] Yuntian Yang[+],[a] Yanqiu Wang,[b] Tie Chen,[a] Long Yi Jin,*[a] and Myongsoo Lee*[b]

Abstract: Amphiphilic coil-rod-coil molecules, incorporating flexible and rigid blocks, have a strong affinity to self-organize into various supramolecular aggregates in bulk and in aqueous solutions. In this paper, we report the self-assembling behavior of amphiphilic coil-rod-coil molecular isomers. These molecules consist of biphenyl and phenyl units connected by ether bonds as the rod segment, and poly(-ethylene oxide) (PEO) with a degree of polymerization of 7 and 12 as the flexible chains. Their aggregation behavior was investigated by differential scanning calorimetry, thermal optical polarized microscopy, small-angle X-ray scattering spectroscopy, and transmission electron microscopy. The results imply that the molecular structure of the rod building block and the length of the PEO chains dramatically influence the creation of supramolecular aggregates in bulk and in aqueous solutions. In the bulk state, these molecules self-organize into a hexagonal perforated lamellar and an oblique columnar structure, respectively, depending on the sequence of the rod building block. In aqueous solution, the molecule with a linear rod segment self-assembles into sheet-like nanoribbons. In contrast, its isomer, with a rod building block substituted at the *meta*-position of the aryl group, self-organizes into nanofibers. This is achieved through the control of the non-covalent interactions of the rod building blocks.

Introduction

The spontaneous organization of organic molecules or block polymers by the orchestrated interplay of various non-covalent interactions has been one of the major research topics in the field of supramolecular chemistry.[1] Among the polymer scaffolds, amphiphilic block copolymers consisting of hydrophobic and hydrophilic blocks can self-assemble into various core-shell nanoaggregates such as spheres, cylinders, fibers, ribbons, and vesicles through aqueous self-assembly.[2] These aggregates incorporate a specific building block with desired functions and act as novel functional nanomaterials. Thus, they have remarkable potential in fields such as biochemistry, molecular electronics, biomimetic chemistry, and materials science.[3] Rod-coil molecules have a strong tendency to form anisotropic and orientational nanostructures that arise from microphase separation of the rod and coil segments. These molecules are spontaneously held together by non-covalent molecular interactions, including hydrophobic and hydrophilic effects, π–π stacking, hydrogen bonding, and electrostatic interactions.[4] We have previously reported that dumbbell-shaped rod-coil molecules with conjugated rod building blocks and hydrophilic dendrons can form helical nanostructures in aqueous solutions.[5] This is achieved through steric repulsion interactions between the parallel arrangement of the conjugated rod block and the bulky dendritic poly(ethylene oxide) (PEO) coil chains. In subsequent work, we synthesized laterally grafted and elliptical macrocycle rod-coil molecules, and constructed 2D porous, closed porous sheets and helical fibers, respectively.[6] Recently, we have reported that depending on the PEO chain lengths in the solid state and aqueous solutions, bent-shaped amphiphilic molecules (consisting of a dibenzo[a,c]phenazine unit as the rigid segment and PEO flexible chains) self-assemble into oblique columnar structures, and cylindrical micelles and helical fibers, respectively.[7] More recently, we have reported the self-assembling behavior of coil-rod-coil molecules incorporating lateral hydroxy or methoxy groups in the center rod segments, and PEO as the coil segments.[8] These molecules aggregate into nanoribbons and vesicles, depending on their lateral groups and oligo(ethylene oxide) chain lengths in aqueous solutions. The above results

[a] *Z. Li,[+] Y. Yang,[+] T. Chen, Prof. L. Y. Jin*
Key Laboratory for Organism Resources of the Changbai Mountain and Functional Molecules, Ministry of Education
Department of Chemistry
Yanbian University
Yanji 133002 (China)
E-mail: lyjin@ybu.edu.cn

[b] *Y. Wang, Prof. M. Lee*
State Key Lab of Supramolecular Structure and Materials
College of Chemistry
Jilin University
Changchun 130012 (China)
E-mail: mslee@jlu.edu.cn

[+] *These authors contributed equally to this work.*

Supporting information for this article can be found under http://dx.doi.org/10.1002/asia.201600683.

indicated that the shape of the rod building block and the lateral groups in the center of the rod segments significantly influence the self-assembly of the rod-coil molecular system in the bulk state and in aqueous solution. This is achieved through the tuning of the driving force of the molecular aggregation.

To our knowledge, the synthesis and self-assembly of coil-rod-coil molecular isomers, based on sequence of the rod building block and the length of the oligo(ethylene oxide) chain in aqueous solution, has not been reported to date. Therefore, it is of great interest to investigate the self-assembly of rod-coil molecular isomers in the bulk state and in aqueous solution to construct various supramolecular nanoaggregates that can be applied to drug delivery systems and nanomaterials science.

With this in mind, we have designed and synthesized coil-rod-coil molecules **1a,b** and **2a,b**, consisting of biphenyl and phenyl units linked together with ether bonds as the rod segments, and PEO with a degree of polymerization (DP) of 7 and 12 as the coil segments (Scheme 1). The rod building blocks of molecules **1a,b**, consist of a *p*-phenyl unit at the center of the rod segment and another two *p*-phenyl groups connected to biphenyl units through ether bonds. The isomers of **1a,b**, namely, *meta*-position substituted molecules **2a,b** (conformation-stable bent-shaped molecules **2a,b** determined by energy minimized molecular structures through the simulation (Gaussian 09-TD-DFT-B3LYP/6-31G(d)) of **2a**–**2b**, see Figure S1), are composed of an *m*-phenyl unit at the center of the rod segments, and *p*-phenyl and biphenyl units, respectively. The self-assembling behavior of these molecules in bulk and in aqueous solution was investigated by using differential scanning calorimetry (DSC), thermal optical polarized microscopy (POM), small-angle X-ray scattering (SAXS), ultraviolet-visible and fluorescence (UV/Vis and FL, respectively) spectroscopy, and transmission electron microscopy (TEM).

Results and Discussion

Molecular Design and Synthesis

Coil-rod-coil triblock molecules **1a,b** and **2a,b**, incorporating phenyls, biphenyls, and a *p*-phenyl or an *m*-phenyl unit linked together with ether bonds as the rod segment, and PEO with a DP of 7 and 12 as the coil segments were synthesized. Poly(ethylene glycol) methyl ether; 1,4-benzenediol; or 1,3-benzenediol were used as the starting materials. Molecules **1a,b** and **2a,b** were afforded from a substitution reaction of compound **4a,b** with 1,4-benzenediol or 1,3-benzenediol in the presence of potassium carbonate. The structures of these molecules were characterized by ^{1}H NMR spectroscopy and matrix-assisted laser desorption ionization time-of-flight (MALDI-TOF) mass spectroscopy (Figures S2 and S3, respectively). All the results were in full agreement with the structures presented in Scheme 1.

Structure Analysis of 1a,b and 2a,b in Bulk State

The self-assembling behavior of coil-rod-coil triblock molecules **1a,b** and **2a,b** was investigated by means of DSC, POM, and SAXS. The transition temperatures of these molecules, determined from the DSC heating and cooling traces (Figure 1), decrease as the PEO coil length increases (Table S1).

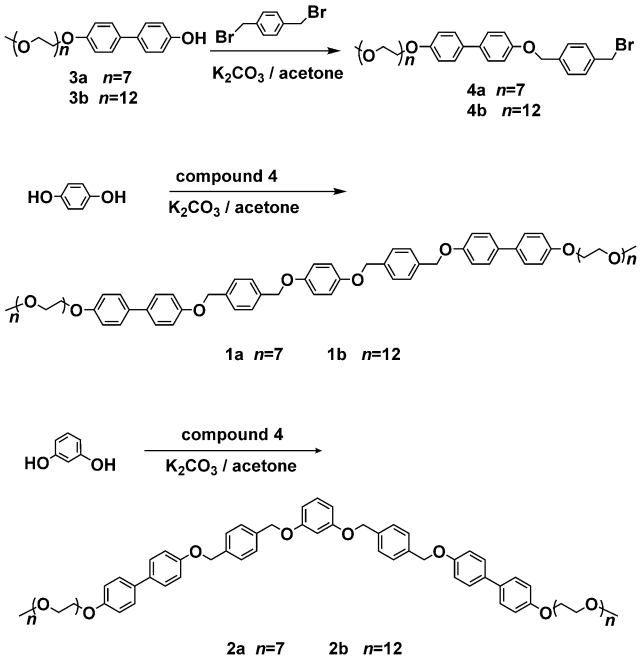

Scheme 1. Synthetic route to molecules **1a,b** and **2a,b**.

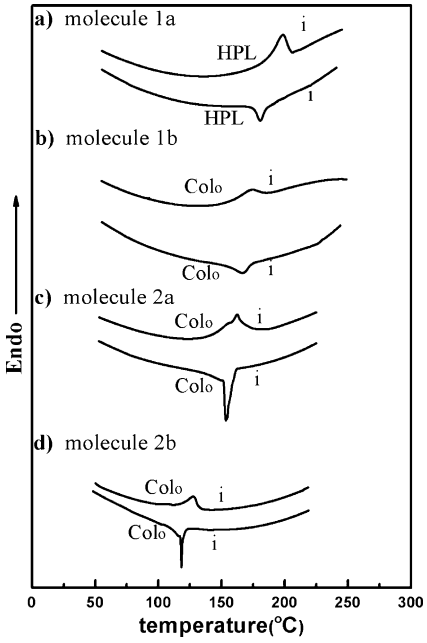

Figure 1. DSC traces (10 °C min^{-1}) recorded during the heating and cooling scans of **1a,b** and **2a,b** (Colo: oblique columnar; HPL: hexagonal perforated lamella; i: isotropic phase).

Interestingly, the transition temperatures of linear molecules **1a,b** are significantly higher than those of *meta*-position substituted molecules **2a,b**. This is indicative of loose stacking of the molecules **2a,b** when compared to the linear molecules. On slow cooling of **1a,b** and **2a,b** from isotropic liquid to room temperature, POM displayed a focal conical fan texture with arced striations, or a spherulitic fan texture. The DSC curves, together with the optical textures, preliminarily confirmed the presence of an ordered columnar phase or hexagonal perforated layer phase (Figure 2 and Figure S4).[9]

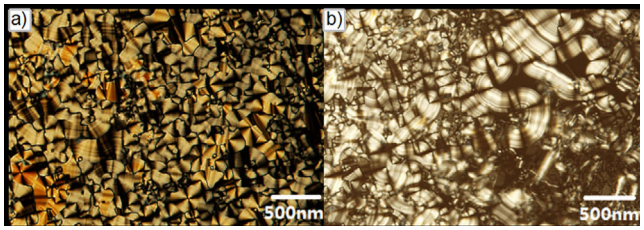

Figure 2. Representative optical polarized micrographs (40×) of the textures exhibited by a) the hexagonal perforated lamellar structure for **1a** at 175 °C and b) the oblique columnar structure for **1b** at 155 °C.

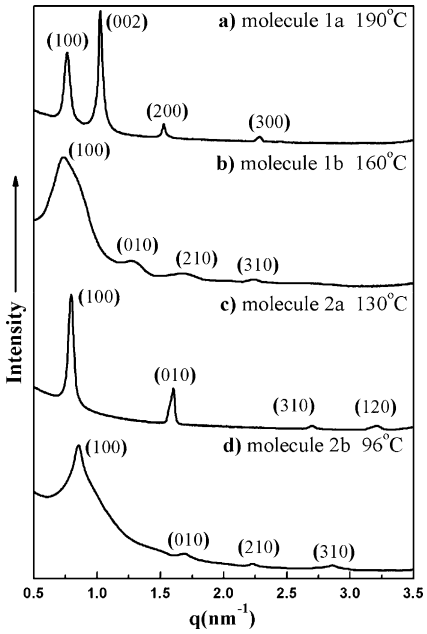

Figure 3. SAXS diffraction patterns of **1a,b** and **2a,b** measured at different temperatures: a) hexagonal perforated lamellar structure for **1a** at 190 °C; b) oblique columnar structure for **1b** at 160 °C; c) oblique columnar structure of **2a** at 130 °C; and d) oblique columnar structure of **2b** at 96 °C.

To identify the detailed self-organizing structures of molecules **1** and **2**, SAXS experiments were performed in the crystalline phases. The SAXS patterns of **1a** display four sharp reflections that can be indexed as the (100), (002), (200), and (300) reflections of a 2D hexagonal perforated lamellar phase with lattice parameters $a=9.5$ nm, $c=12.3$ nm. An interesting point is that the peak intensity associated with the (002) reflection of molecule **1a** appears to be the most intense, implying that the fundamental structure is lamellar. Therefore, we confirm that molecule **1a** self-organizes into a hexagonally perforated lamellar structure in the crystalline phase.

The result of SAXS analysis is consistent with POM experiment (Figure S4). Meanwhile, the WAXS pattern of molecule **1a** shows four clear peaks at q-spacings of 9.55, 11.91, 14.24, and 17.15 nm^{-1}, which appear due to crystal packing of the rod segments within the aromatic domain. The molecules pack in a rectangular lattice with unit cell dimensions of $a=8.8$ Å and $b=6.5$ Å (Figure S5). For molecule **1b**, the SAXS patterns display four sharp reflections that can be indexed as the (100), (010), (210), and (310) reflections with lattice parameters $a=8.8$ nm, $b=5.2$ nm, and $\gamma=74.5°$. These characteristic peaks, together with the POM images, imply the existence of a hexagonal perforated lamellar phase and an oblique columnar phase as the crystalline mesophase of molecules **1a** and **1b**, respectively.[10] Similarly, coil-rod-coil molecules **2a** and **2b**, based on a bent-shaped rod segment, display an oblique columnar structure with lattice parameters $a=8.0$ nm, $b=3.9$ nm, $\gamma=83°$ and $a=7.4$ nm, $b=3.8$ nm, $\gamma=82°$, respectively (Figure 3 and Table S2).[11] Similar to molecule **1a**, the WAXS pattern of molecules **1b**, **2a**, and **2b** also exhibit three clear reflections, which can be assigned as a rectangular structure with lattice parameters $a=8.9$ Å, $b=6.7$ Å for **1b**, $a=9.0$ Å, $b=6.8$ Å for **2a** and $a=9.2$ Å, $b=6.9$ Å for **2b**, respectively (Figure S5).This result demonstrates that these molecules are highly packed within the rod segments of the rod-coil molecules.

Notably, molecules **1a** and **1b**, having the same rod segment but a different PEO coil length, self-organize into a hexagonal perforated lamellar or an oblique columnar structure (Figure 4), depending on the coil-chain length. On the other hand, *meta*-position substituted **2a** and **2b** self-assemble into oblique columnar structures in the solid state. Clearly, the diverse volume fractions of the flexible chains and the sequence of the rod segments lead to the construction of different supramolecular nanostructures. This is mainly due to the relatively loose packing of molecules **2a** and **2b** (when compared to that of their corresponding linear isomers **1a** and **1b**), and is caused by steric hindrance of the bent-shaped rod building blocks and the coil-chain length.

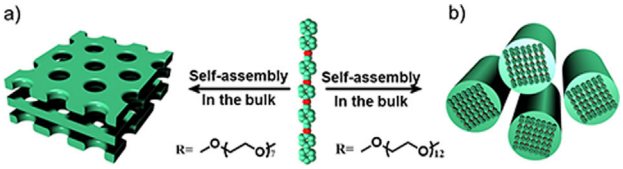

Figure 4. Schematic representation of self-assembly of **1a,b** in bulk state. a) A hexagonal perforated lamellar structure of **1a.** b) An oblique columnar structure of **1b**. PEO chains are not shown.

Aggregation Behavior in Aqueous Solution

Molecules **1a,b** and **2a,b** consist of a hydrophilic flexible PEO chain and a hydrophobic rigid aromatic segment. When dissolved in water, they can self-assemble into an ordered aggre-

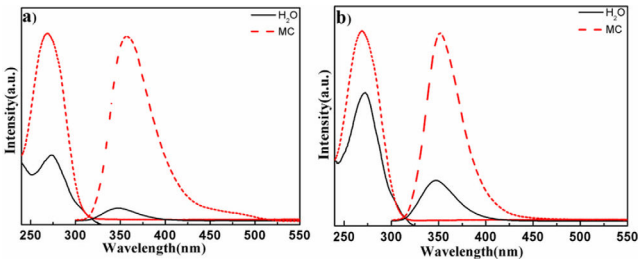

Figure 5. Absorption and emission spectra of **2a**,**b** in methylene chloride (MC) and aqueous solution (2×10^{-5} M) a) **2a**; b) **2b**.

gate due to their amphiphilic characteristics.[12] The aggregation behavior of these molecules was subsequently studied in dichloromethane and aqueous solutions by UV/Vis and FL spectroscopy. The absorption spectra of **2a** and **2b** in aqueous solution (5×10^{-5} M) exhibit a red-shift in the absorption maxima compared to those in dichloromethane solution. This is a result of the conjugated rod block (Figure 5).

These observations may be caused by the cooperative effect between the hydrophilic and hydrophobic interactions, and the π–π stacking interactions between the aromatic segments.[13] The fluorescence spectrum of **2a** in dichloromethane solution (Figure 5) exhibits a strong emission maximum at 348 nm. However, the emission maximum in aqueous solution is blue-shifted with respect to that observed in the chloroform solution, and the fluorescence is significantly quenched. This implies an aggregation of the conjugated rod segments. The same phenomena were also observed in the UV/Vis and FL spectra of **1a**,**b** (Figure S6). The dynamic light scattering(DLS) experiments further corroborated this; the DLS data show that molecules **1** and **2** self-assemble into nano-aggregates with average hydrodynamic diameters ranging from 35 to 142 nm (Figure S7).[13c]

Evidence for the creation of supramolecular aggregates in dilute aqueous solution was also provided by TEM (Figure 6). The micrograph of a sample cast from an aqueous solution of

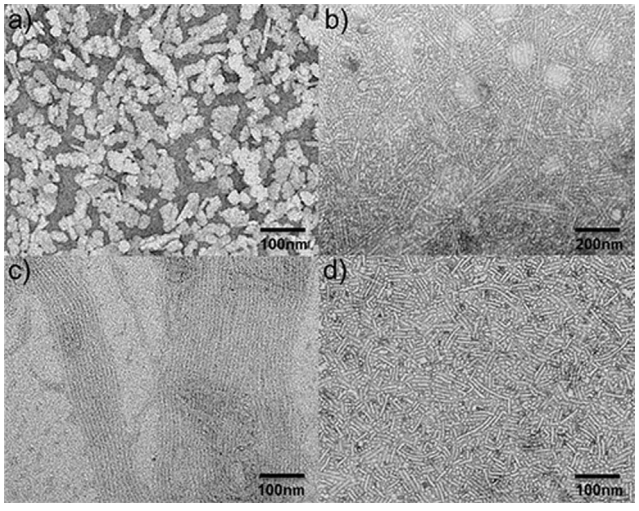

Figure 6. TEM images of negatively stained nanoaggregates a) **1a**; b) **1b**; c) **2a**; d) **2b** (obtained from 5×10^{-5} M aqueous solution).

compound **1a** (5×10^{-5} M) and negatively stained with sodium phosphotungstate displayed sheet-like nanoribbons with an average width and length of ~40 and ~200 nm, respectively. Interestingly, **1b**, with a longer PEO chain than **1a**, exhibits short nanofibers with lengths up to ~300 nm and a uniform diameter of ~13.0 nm. The fully extended molecular length of **1b**, estimated by CPK modeling to be 14.1 nm, is similar to the measured length. Thus, we deduced that the cylindrical entity, formed from aqueous solution, consists of a rigid rod building block and a hydrophilic PEO chain that are surrounded by rod segments and are fully interdigitated with each other. This result indicates that an increase in the length of the hydrophilic PEO chain increases the interfacial curvature. Thus, compound **1b** favors self-organization into the relatively more dynamically stable nanofibers over the formation of nanoribbons. This construction of various supramolecular nanostructures can also be explained by considering the relative volume fraction of the hydrophobic rod segments to hydrophilic PEO head groups.

In contrast to molecules **1a**,**b**, the TEM images of bent-shaped molecules **2a**,**b**, with an *m*-phenylene unit at the center of the rod segment, display supramolecular nanofibers and cylindrical micelles, depending on the length of the PEO chains. Molecule **2a**, with a PEO DP of 7, spontaneously self-assembles into nanofibers with a uniform diameter of ~6.5 nm and average lengths up to several micrometers. To further corroborate the construction of nanofibers of molecule **2a** in aqueous solution, we performed a cryo-TEM investigation. As shown Figure S8, the micrograph shows the nanofiber with uniform diameters against the vitrified aqueous solution background. On the other hand, molecule **2b**, with a longer PEO chain, self-organizes into short-length cylindrical micelles with a uniform diameter of ~10.0 nm and a length of ~120 nm (Figure 6d). The fully extended molecular lengths of both rod and coil blocks of molecules **2a**,**b** (estimated to be 7.1 and 11.9 nm, respectively, by CPK modeling) are less than those of the observed diameters. These results indicate that the cylindrical entities consist of hydrophobic aromatic inner cores surrounded by hydrophilic flexible PEO segments that are exposed to the aqueous environment (Figure 6). Similar to the construction of various molecular aggregates of molecules **1a**,**b**, the volume fraction of the hydrophilic PEO head groups of **2a**,**b** significantly influences the formation of the ordered nanoentities by the tuning of the interfacial area between the hydrophilic and hydrophobic domains. Therefore, the effective hydrophilic coil ratio of the rod-coil amphiphilic molecules gives rise to the formation of ordered supramolecular nanoassemblies.

It should be pointed out that molecules **1a** and **2a** have the same molecular weight and PEO coil segments, but a different sequence of rod building blocks. Molecule **1a**, with a linear-shaped rod segment, self-assembles into sheet-like nanoribbons in dilute aqueous solutions. However, molecule **2a**, with a *meta*-position substituted aromatic rod segment, self-organizes into nanofibers. A similar tendency of the self-organization of **1b** and **2b** into short nanofibers and cylindrical micelles was also observed by TEM experiments. The results of the self-

assembling behavior of these isomers imply that the sequence of the rod building block is also the main parameter that influence the creation of supramolecular nanoassemblies of rod-coil molecular systems in an aqueous environment. This is consistent with the self-assembling behavior of the linear rod-coil isomers reported by our team in bulk state. The variation of aggregate morphology might be partly explained by the sequence of the individual molecules and the effective cross sectional area of the hydrophilic head groups. Although molecules **1a** and **2a** have the same effective hydrophilic domains, a second driving force of linear **1a** might be responsible for the strong π–π interactions between the aromatic segments down the perpendicular surface of the sheet-like ribbons, demonstrated in bulk state. Thus, the interface of **1a** between the hydrophilic rod segment and the hydrophobic coil domains is flatter than that of **2a**. This causes a small interfacial area and results in the formation of more dynamic stable sheet-like assemblies.

On the basis of the above discussion, we have concluded that molecules **1a** and **2a** self-assemble into nanosheet-like aggregates and long nanofibers in aqueous solution, respectively (Figure 7). However, molecules **1b** and **2b**, with longer

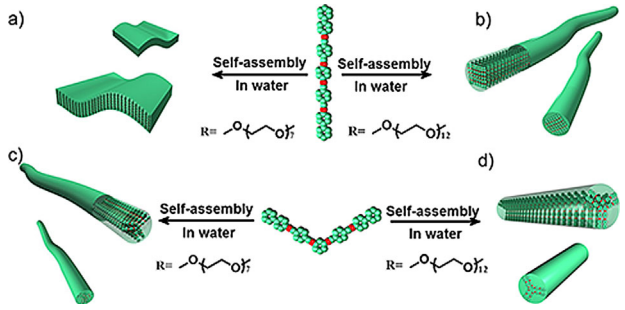

Figure 7. Schematic representation of the proposed self-assembly of molecules in aqueous solution: a) nanoribbons for **1a**; b) short nano-fibers for **1b**; c) nano-fibers **2a**; d) cylindrical micelles for **2b**. PEO chains are not shown.

PEO chains, self-assemble into short nanofibers and cylindrical micelles, respectively, in a dilute aqueous environment. Although these molecules have the same rod and coil segments, they have a different rod shape and sequence of rod building blocks. This is caused by the cooperative effect between the hydrophilic and hydrophobic interactions, and the π–π stacking interactions between the aromatic segments. This effect is the driving force for the self-assembly of the rod segments into ordered nanostructures.

Conclusions

Amphiphilic coil-rod-coil triblock molecules **1a,b** and **2a,b**, incorporating biphenyl and phenyl units connected together with ester bonds as a rod segment and PEO with a DP of 7 and 12, were synthesized. Their self-assembling behavior was investigated in bulk state and in aqueous solution. In the bulk state, these molecules self-organize into a hexagonal perforated lamellar and an oblique columnar structure, respectively, depending on the sequence of the rod building block. In aqueous solution, molecule **1a**, with a linear rod segment, self-assembles into sheet-like nanoribbons, whereas the isomer of molecule **1a** (**2a**) with *meta* substitution of the central C_6H_4 group, self-organizes into nanofibers through the control of the non-covalent interactions of the rod building blocks. The experimental results described herein imply that the sequence of the rod building block and the length of the PEO chains dramatically influence the creation of supramolecular aggregates in bulk and aqueous solutions. Notably, the non-covalent driving force of the molecular architecture of differently shaped rod-coil molecules can be tuned precisely to construct diverse supramolecular functional materials. These materials can be applied to drug delivery systems and biomolecular sensors.

Experimental Section

General Materials: Poly(ethylene glycol) methyl ether (M_W = 350,550), toluene-*p*-sulfonyl chloride (99%), 4,4′-biphenol, 1-(dibromomethyl)-4-methylbenzene, 1,4-benzenediol (99%), 1,3-benzenediol, pyridine, potassium carbonate (Aldrich, TCI, and Alfa Aesar, etc.) and conventional reagents were used as received. Compounds **3** and **4** were prepared according to the references described elsewhere (see the Supporting Information).[14]

Characterization: Flash column chromatography was performed using silica gel (200–300 mesh). ^{1}H NMR(300 MHz) was recorded in $CDCl_3$ on Bruker AM-300 instruments. Chemical shifts were described in parts per million (ppm, δ units) downfield of tetramethylsilane (TMS) as an internal standard. MALDI-TOF-MS was performed on a PerSeptive Biosystems Voyager-DESTR using 2-cyano-3-(4-hydroxyphenyl) acrylic acid (CHCA) as the matrix. A PerkinElmer Pyris Diamond differential scanning calorimeter was used to determine the thermal transitions, which were reported as the maxima and minima of their endothermic or exothermic peaks; the heating and cooling rates were controlled to 10 °C min^{-1} under a N_2 atmosphere. An Olympus optical polarized micro scope, equipped with a Mettler FP 82 hot-stage and a Mettler FP 90 central processor, was used to observe the thermal transitions and to analyze the anisotropic texture. The SAXS measurements were performed in transmission mode with synchrotron radiation at the 1W2A X-ray beam line at Beijing Accelerator Laboratory.[15] The UV/Vis and fluorescence spectra were obtained from a Shimadzu UV-1650PC spectrometer and a Hitachi F-4500 fluorescence spectrometer, respectively. Transmission electron microscopy (TEM) was performed with a JEOL JEM-2100F microscope.

General Synthetic Procedure for 1 and 2: Coil-rod-coil molecules **1a,b** and **2a,b** were synthesized with similar procedures. A representative example is described here for **1a**. Compound **4a** (0.3 g, 0.43 mmol) and potassium carbonate (98 mg, 0.71 mmol) were dissolved in 40 mL acetone. Next, 1,4-benzenediol (0.016 g, 0.14 mmol) was added dropwise to the mixture and heated at reflux for 24 h. The resulting solution was filtered and concentrated, and the crude product was purified by column chromatography (silica gel, CH_2Cl_2, ethyl acetate and CH_2Cl_2:CH_3OH = 20:1) to yield 0.14 g (74.0%) white solid.

^{1}H NMR (300 MHz,$CDCl_3$): δ = 7.47–7.62 (m,16Ar-H, *o* to phenyl-OCH_2CH_2O, *o* to phenylOCH_2, *o* to CH_2Ophenyl), 6.96–7.16 (m, 12Ar-H, *m* to phenylOCH_2CH_2O, *m* to phenylOCH_2, *o* to

OCH_2phenyl), 5.14 (s, 8H,OCH_2phenyl), 4.16 (t, 4H, phenyl-OCH_2CH_2O), 3.87(t, 4H, phenyl-OCH_2CH_2O), 3.55–3.72(m,48H, -OCH_2CH_2O-), 3.37 ppm (s, 6H, OCH_3). MALDI-TOF-MS *m/z* $[M]^+$ 1331, $[M+Na]^+$ 1354.

1b: white solid (75.0%).^{1}H NMR (300 MHz, $CDCl_3$): $\delta = 7.47–7.62$ (m,16Ar-H, *o* to phenylOCH_2CH_2O, *o* to phenylOCH_2, *o* to CH_2Ophenyl), 6.96–7.16 (m, 12Ar-H, *m* to phenylOCH_2CH_2O, *m* to phenylOCH_2, *o* to OCH_2phenyl), 5.14 (s, 8H,OCH_2phenyl), 4.16 (t, 4H, phenyl-OCH_2CH_2O), 3.87 (t, 4H, phenyl-OCH_2CH_2O), 3.55–3.72 (m,88H, -OCH_2CH_2O-), 3.37 ppm (s, 6H, OCH_3). MALDI-TOF-MS *m/z* $[M]^+$ 1772, $[M+Na]^+$ 1795.

2a: white solid (72.0%). ^{1}H NMR (300 MHz,$CDCl_3$): $\delta = 7.47–7.62$ (m,16Ar-H, *o* to phenylOCH_2CH_2O, *o* to phenyl OCH_2, *o* to CH_2Ophenyl), 7.23 (t,1Ar-H) 6.96–7.16 (m, 8Ar-H, *m* to phenyl-OCH_2CH_2O, *m* to phenylOCH_2), 6.35–6.60 (3Ar-H), 5.14 (s, 8H,OCH_2phenyl), 4.16 (t, 4H, phenyl-OCH_2CH_2O), 3.87 (t, 4H, phenyl-OCH_2CH_2O), 3.55–3.72 (m,48H, -OCH_2CH_2O-), 3.37 ppm (s, 6H, OCH_3). MALDI-TOF-MS *m/z* $[M]^+$ 1331.

2b: white solid (71.0%). ^{1}H NMR (300 MHz,$CDCl_3$): $\delta = 7.47–7.62$ (m,16Ar-H, *o* to phenylOCH_2CH_2O, *o* to phenyl OCH_2, *o* to CH_2Ophenyl, 7.23 (t, 1Ar-H), 6.96–7.16 (m, 8Ar-H, *m* to phenyl-OCH_2CH_2O, *m* to phenylOCH_2), 6.35–6.60 (3Ar-H), 5.1 (s, 8H,OCH2-phenyl), 4.16 (t, 4H, phenyl-OCH_2CH_2O), 3.87 (t, 4H, phenyl-OCH_2CH_2O), 3.55–3.72 (m, 88H, -OCH_2CH_2O-), 3.37 ppm (s, 6H, OCH_3). MALDI-TOF-MS *m/z* $[M]^+$ 1772.

Acknowledgements

This work was supported by the National Natural Science Foundation of China (grant number: 21562043, 21564016, 21164013), the Open Projects of the State Key Laboratory of Supramolecular Structure and Materials (sklssm201430), Jilin University, China. We are grateful to Bejing Synchrotron Radiation Facility (BSRF), Institute of High Energy Physics, Chinese Academy of Sciences for help with the X-ray scattering measurements of molecular structures.

Keywords: amphiphiles · coil-rod-coil structures · nanofibers · nanostructures · self-assembly

[1] a) M. Huang, C. Hsu, J. Wang, S. Mei, X. Dong, Y. Li, M. Li, H. Liu, W. Zhang, T. Aida, W. Zhang, K. Yue, S. Z. D. Cheng, *Science* **2015**, *348*, 424–428; b) B. A. G. Hammer, K. Müllen, *Chem. Rev.* **2016**, *116*, 2103–2140; c) T. F. A. De Greef, M. M. J. Smulders, M. Wolffs, A. P. H. J. Schenning, R. P. Sijbesma, E. W. Meijer, *Chem. Rev.* **2009**, *109*, 5687–5694; d) M. Garzoni, K. Okuro, N. Ishii, T. Aida, G. M. Pavan, *ACS Nano* **2014**, *8*, 904–914; e) G. Yu, K. Jie, F. Huang, *Chem. Rev.* **2015**, *115*, 7240–7303; f) B. Yuan, H. Yang, Z. Q. Wang, X. Zhang, *Langmuir* **2014**, *30*, 15462–15467; g) Z. Huang, S.-K. Kang, M. Banno, T. Yamaguchi, D. Lee, C. Seok, E. Yashima, M. Lee, *Science* **2012**, *337*, 1521–1527; h) A. Wang, W. Shi, J. Huang, Y. Yan, *Soft Matter* **2016**, *12*, 337–342; i) A. Tena, A. Marcos-Fernandez, M. de La Viuda, L. Palacio, P. Pradanos, A. E. Lozano, J. de Abajo, A. Hernandez, *Eur. Polym. J.* **2015**, *62*, 130–138; j) Y. Wang, X. Gao, Y. Xiao, Q. Zhao, J. Yang, Y. Yan, J. Huang, *Soft Matter* **2015**, *11*, 2806–2811.

[2] a) Y. Mai, A. Eisenberg, *Chem. Soc. Rev.* **2012**, *41*, 5969–5974; b) R. C. Hayward, D. J. Pochan, *Macromolecules* **2010**, *43*, 3577–3584; c) L. Chen, H. Chen, X. Yao, X. Ma, H. Tian, *Chem. Asian J.* **2015**, *10*, 2352–2357; d) X. Tan, L. Yang, Z. Huang, Y. Yu, Z. Wang, X. Zhang, *Polym. Chem.* **2015**, *6*, 681–685; e) Y. Kim, M. Lee, *Chem. Eur. J.* **2015**, *21*, 5736–5740; f) H. Kim, Y. Kim, S. Cho, M. Lee, *Chem. Eur. J.* **2015**, *21*, 11836–11842; g) I.-S. Park, Y.-R. Yoon, M. Jung, K. Kim, S. B. Park, S. Shin, Y.-B. Lim, M. Lee, *Chem. Asian J.* **2011**, *6*, 452–458; h) D. Vlassopoulos, G. Fytas, *Macromolecules* **2016**, *49*, 3516–3525.

[3] a) A. Rösler, G. W. M. Vandermeulen, H.-A. Klok, *Adv. Drug Delivery Rev.* **2012**, *64*, 270–276; b) H.-J. Kim, T. Kim, M. Lee, *Acc. Chem. Res.* **2011**, *44*, 72–82; c) X. Yan, T. R. Cook, P. Wang, F. Huang, P. J. Stang, *Nat. Chem.* **2015**, *7*, 342–348; d) Y. Wang, Z. Huang, Y. Kim, Y. He, M. Lee, *J. Am. Chem. Soc.* **2014**, *136*, 16152–16155; e) Y. Yamamoto, T. Fukushima, Y. Suna, N. Ishii, A. Saeki, S. Seki, S. Tagawa, M. Taniguchi, T. Kawai, T. Aida, *Science* **2006**, *314*, 1761–1764; f) S. S. Babu, V. K. Praveen, A. Ajayaghosh, *Chem. Rev.* **2014**, *114*, 1973–2129.

[4] a) Y. Yan, B. Li, W. Li, H. Li, L. Wu, *Soft Matter* **2009**, *5*, 4047–4053; b) S. Chen, C. Ma, Z. Huang, M. Lee, *J. Phys. Chem. C* **2014**, *118*, 8181–8186; c) J. Zhu, K. Zhong, Y. Liang, Z. Wang, T. Chen, L. Y. Jin, *Tetrahedron* **2014**, *70*, 1230–1235; d) S. Yagai, Y. Nakano, S. Seki, A. Asano, T. Okubo, T. Isoshima, T. Karatsu, A. Kitamura, Y. Kikkawa, *Angew. Chem. Int. Ed.* **2010**, *49*, 9990–9994; *Angew. Chem.* **2010**, *122*, 10186–10190; e) E. Lee, Z. Huang, J.-H. Ryu, M. Lee, *Chem. Eur. J.* **2008**, *14*, 6957–6966.

[5] a) J.-H. Ryu, H.-J. Kim, Z. Huang, E. Lee, M. Lee, *Angew. Chem. Int. Ed.* **2006**, *45*, 5304–5307; *Angew. Chem.* **2006**, *118*, 5430–5433; b) Z. Huang, S.-K. Kang, M. Lee, *J. Mater. Chem.* **2011**, *21*, 15327–15331.

[6] a) Y. Kim, S. Shin, T. Kim, D. Lee, C. Seok, M. Lee, *Angew. Chem. Int. Ed.* **2013**, *52*, 6426–6429; *Angew. Chem.* **2013**, *125*, 6554–6557; b) J. K. Kim, E. Lee, M.-C. Kim, E. Sim, M. Lee, *J. Am. Chem. Soc.* **2009**, *131*, 17768–17770.

[7] Y. Liu, K. L. Zhong, Z. H. Li, Y. Q. Wang, T. Chen, M. Lee, L. Y. Jin, *Polym. Chem.* **2015**, *6*, 7395–7401.

[8] Z. Lu, K. Zhong, Y. Liu, Z. Li, T. Chen, L. Y. Jin, *Soft Matter* **2016**, *12*, 3860–3867.

[9] a) K. L. Zhong, Z. Man, Z. Huang, T. Chen, B. Yin, L. Yi Jin, *Polym. Int.* **2011**, *60*, 845–850; b) P. F. Duan, H. Cao, L. Zhang, M. H. Liu, *Soft Matter* **2014**, *10*, 5428.

[10] a) L. Yi Jin, J. Bae, J. Ahn, M. Lee, *Chem. Commun.* **2005**, *9*, 1197–1199; b) Z. Wang, K. Zhong, Y. Liang, T. Chen, B. Yin, M. Lee, L. Y. Jin, *J. Polym. Sci. Part A* **2015**, *53*, 85–92; c) C. Grigoriadis, G. Zardalidis, R. Graf, H.-J. Butt, G. Floudas, *Macromolecules* **2014**, *47*, 5691–5702.

[11] Z. Wang, J. Cui, Y. Liang, T. Chen, M. Lee, B. Yin, L. Y. Jin, *J. Polym. Sci. Part A* **2013**, *51*, 5021–5028.

[12] a) W. Li, Y. Kim, J. Li, M. Lee, *Soft Matter* **2014**, *10*, 5231–5242; b) K. Zhang, J. Tian, D. Hanifi, Y. Zhang, A. C. Sue, T.-Y. Zhou, L. Zhang, X. Zhao, Y. Liu, Z.-T. Li, *J. Am. Chem. Soc.* **2013**, *135*, 17913–17918; c) W. Li, Y. Kim, M. Lee, *Nanoscale* **2013**, *5*, 7711–7723; d) G. Zhang, W. Jin, T. Fukushima, A. Kosaka, N. Ishii, T. Aida, *J. Am. Chem. Soc.* **2007**, *129*, 719–722; e) M. H. Liu, L. Zhang, T. Y. Wang, *Chem. Rev.* **2015**, *115*, 7304–7397; f) X. Tan, Z. Wang, X. Zhang, *Chem. Rev.* **2015**, *115*, 7196–7239.

[13] a) K.-L. Zhong, Q. Wang, T. Chen, L. Y. Jin, *Eur. Polym. J.* **2013**, *49*, 3244–3250; b) M. Lee, C. J. Jang, J. H. Ryu, *J. Am. Chem. Soc.* **2004**, *126*, 8082–8083; c) K. Wunderlich, A. Larsen, J. Marakis, G. Fytas, M. Klapper, K. Müllen, *Small* **2014**, *10*, 1914–1919.

[14] S. Yu, Y. Yang, C. Li, T. Chen, L. Y. Jin, *Polym. Int.* **2015**, *64*, 1408–1414.

[15] Z. Li, Z. Wu, G. Mo, X. Xing, P. Liu, *Instrum. Sci. Technol.* **2014**, *42*, 128–141.

Manuscript received: May 17, 2016

Accepted Article published: June 27, 2016

Final Article published: ■■ ▮▮, 0000

FULL PAPER

Hot rods: Self-assembling behavior of amphiphilic coil-rod-coil molecular isomers, consisting of biphenyl and phenyl units, incorporating *p*-aryl or *m*-aryl groups in the middle of the rod segments was investigated in bulk and in aqueous solutions. The experimental results suggest that the sequence of the rod building block dramatically influences self-assembly of the rod-coil molecular system.

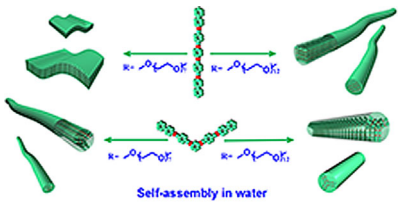

Self-Assembly

Zhaohua Li, Yuntian Yang, Yanqiu Wang, Tie Chen, Long Yi Jin, Myongsoo Lee**

■■ – ■■

Construction of Supramolecular Assemblies from Self-Organization of Amphiphilic Molecular Isomers